

Microwave surface resistance of pristine and neutron-irradiated MgB_2 samples in magnetic field

M. Bonura¹, A. Agliolo Gallitto¹, M. Li Vigni¹, C. Ferdeghini², and C. Tarantini²

¹ CNISM and Dipartimento di Scienze Fisiche e Astronomiche, Università di Palermo, Via Archirafi 36, I-90123 Palermo, Italy

² CNR-INFN-LAMIA and Dipartimento di Fisica, Università di Genova, Via Dodecaneso 33, I-16146 Genova, Italy

the date of receipt and acceptance should be inserted later

Abstract. We report on the microwave surface resistance of two polycrystalline Mg^{11}B_2 samples; one consists of pristine material, the other has been irradiated at very high neutron fluence. It has already been reported that in the strongly irradiated sample the two gaps merge into a single value. The mw surface resistance has been measured in the linear regime as a function of the temperature and the DC magnetic field, at increasing and decreasing fields. The results obtained in the strongly irradiated sample are quite well justified in the framework of a generalized Coffey and Clem model, in which we take into account the field distribution inside the sample due to the critical state. The results obtained in the pristine sample show several anomalies, especially at low temperatures, which cannot be justified in the framework of standard models for the fluxon dynamics. Only at temperatures near T_c and for magnetic fields greater than $0.5H_{c2}(T)$ the experimental data can quantitatively be accounted for by the Coffey and Clem model, provided that the upper-critical-field anisotropy is taken into due account.

PACS. 74.25.Ha Magnetic properties – 74.25.Nf Response to electromagnetic fields (nuclear magnetic resonance, surface impedance, etc.) – 74.25.Op Mixed states, critical fields, and surface sheaths

1 Introduction

It has widely been shown that the superconducting properties of MgB_2 are strongly related to the two-gap structure of its electronic states [1,2,3,4,5,6]. The smaller superconducting gap, Δ_π , arises from the quite isotropic π bands and the larger one, Δ_σ , from the strongly anisotropic σ bands [7]. Due to the different parity of the σ and π bands, inter-band scattering of quasiparticles is much smaller than the intra-band one, making the two superconducting gaps quite different though they close at the same T_c [8].

According to the theory of multi-band superconductivity [7], the inclusion of defects would increase the inter-band scattering and, consequently, change the relative magnitude of the different gaps. In order to carry out investigation on this topic, essentially two methods have been used to insert defects and/or disorder in MgB_2 : chemical substitution and damage by irradiation [9,10,11,12,13]. In any cases, the inclusion of defects, besides to change the inter-band scattering, might increase the upper critical field and the critical current, strongly affecting the fluxon dynamics. Very recently, the effects of neutron irradiation have extensively been investigated on polycrystalline Mg^{11}B_2 [13,14,15,16,17]. It has been shown that irradiation leads to an improvement in both critical field and critical current density for an exposure level in the range $1 \div 2 \times 10^{18} \text{ cm}^{-2}$. On further increasing the neu-

tron fluence, all the superconducting properties, such as T_c , H_{c2} , J_c , are strongly suppressed. Furthermore, measurements of specific heat, as well as point-contact spectroscopy, have shown that in the sample irradiated at the highest fluence ($1.4 \times 10^{20} \text{ cm}^{-2}$) the two gaps merge into a single value [15,16].

Despite the large amount of experimental and theoretical work done on MgB_2 , some arguments are still under discussion, such as the effects of the magnetic field on the superconducting properties [18,19,20]. The main difficulty to quantitatively discuss the mixed-state properties of MgB_2 arises from the unusual flux-line properties due to the different coherence lengths, ξ_σ and ξ_π , associated with Δ_σ and Δ_π [21]. Scanning tunnelling spectroscopy on MgB_2 single crystals along the c -axis, which probes mainly the π band, has highlighted a core size much larger than the estimates based on the measured H_{c2} values, as well as a significant core overlap at fields much lower than the macroscopic H_{c2} [22]. Furthermore, measurements of neutron scattering from the vortex lattice have highlighted a spatial rotation of the vortex lattice for applied magnetic fields in the range $0.5 \div 1 \text{ T}$ [23]. According to point-contact-spectroscopy experiments [24,25,26], these unusual properties have been ascribed to the strong suppression of the superconductivity in the π band, occurring in that field range. At low fields, each vortex has a composite structure, with σ -band quasiparticles local-

ized in a region of radius ξ_σ and π -band quasiparticles in a wider region of radius ξ_π . In the field range $0.5 \div 1$ T (at low T), the giant cores start to overlap; when the magnetic field is large enough to suppress the π -band gap, the vortex cores shrink and the π -band quasiparticles are widespread in the whole sample [19,22]. This field-induced evolution of the vortex lattice is expected to affect the vortex-vortex and vortex-pinning interactions, making the description of the properties involving the presence and motion of fluxons very difficult.

The investigation of the microwave (mw) surface impedance, $Z_s = R_s + iX_s$, in superconductors is a useful tool for determining several properties of the superconducting state. In the absence of static magnetic fields, the variation with the temperature of the condensed-fluid density determines the temperature dependence of Z_s . On the other hand, the field dependence of R_s in superconductors in the mixed state is determined by the presence of fluxons, which bring along normal fluid in their cores, as well as the fluxon motion [27,28,29,30,31,32]. So, investigation of the magnetic-field-induced variations of the surface resistance provides important information on the fluxon dynamics.

Several studies of the mw response of MgB₂ reported in the literature have shown that the experimental results cannot be accounted for in the framework of standard theories [33,34,35,36,37,38,39]. The temperature dependence of the mw conductivity, at zero DC magnetic field, has been justified considering the coexistence of two different superconducting fluids, one related to carriers living on the σ band and the other to carriers living on the π band [33,34]. The magnetic field dependence of the surface resistance has shown an anomalous behavior especially at low temperatures; several authors have highlighted unusually enhanced field-induced mw losses at applied magnetic fields much lower than the upper critical field [35,36,37,38]. Sarti et al. [39], investigating the mw surface impedance of MgB₂ film, have shown that at low fields, when the contribution of the π -band superfluid cannot be neglected, the magnetic-field dependence of the real and imaginary components of the surface impedance exhibits several anomalies. Furthermore, a magnetic hysteresis of unconventional shape has been detected in the $R_s(H)$ curves [38,40]. All these results have suggested that in a wide magnetic-field range the standard models for fluxon dynamics fail when applied to MgB₂.

In this paper, we report on the microwave surface resistance of two of the polycrystalline Mg¹¹B₂ samples studied in Refs. [13,14,15,16,17]. We have investigated the unirradiated sample, which clearly shows two-gap superconductivity, and the sample irradiated at the highest neutron fluence, in which the two gaps merge into a single value. The investigation has been carried out with the aim to compare the results obtained in two-gap and one-gap MgB₂ superconductors. To our knowledge, the mw response of neutron-irradiated MgB₂ samples has not yet been investigated. The mw surface resistance has been measured as a function of the temperature, in the range $2.5 \div 40$ K, and the DC magnetic field, from 0 to 1 T, at increasing and decreasing values. We show that the results

obtained in the strongly irradiated sample can quite well be justified in the framework of standard models, in the whole ranges of temperatures and magnetic fields investigated. On the contrary, the results obtained in the pristine sample cannot thoroughly be justified. In particular, the $R_s(T)$ behavior at zero field has been accounted for, in the framework of the two-fluid model, assuming a linear temperature dependence of the normal and condensed fluid densities. At low temperatures, the field dependence of R_s has shown several anomalies, among which a magnetic hysteresis having a unexpected shape. At temperatures near T_c and applied magnetic fields greater than $\approx 0.5H_{c2}(T)$, the results are well accounted for in the framework of the Coffey and Clem model [30], with fluxons moving in the flux-flow regime, taking into account the anisotropy of the upper critical field.

2 Experimental apparatus and samples

The microwave surface resistance, R_s , has been investigated in two bulk MgB₂ samples. The procedure for the preparation and irradiation of the samples is reported in detail elsewhere [13,16]. The samples have been prepared by direct synthesis from Mg (99.999% purity) and crystalline isotopically enriched ¹¹B (99.95% purity), with a residual ¹⁰B concentration lower than 0.5%. The use of isotopically enriched ¹¹B makes the penetration depth of the thermal neutrons greater than the sample thickness, guarantying the irradiation effect almost homogeneous over the sample. Several superconducting properties of the samples have been reported in Refs. [13,14,15,16,17]. For simplicity and ease of comparison, we label the two samples as in Ref. [13], i.e. P0 (pristine Mg¹¹B₂) and P6 (irradiated at the highest neutron fluence). According to point-contact spectroscopy [15] and specific-heat measurements [16], sample P0 shows a clear two-gap superconductivity; in sample P6 the irradiation process at very high fluence (1.4×10^{20} cm⁻²) determined a merging of the two gaps into a single value.

Sample P0 has a nearly parallelepiped shape with $w \approx 3.1$ mm, $t \approx 1.5$ mm and $h \approx 3.2$ mm; it undergoes a narrow superconducting transition with $T_c^{onset} \approx 39.0$ K and $\Delta T_c \approx 0.2$ K (from 90% to 10% of the normal-state resistivity); its residual normal-state resistivity is $\rho(40$ K) ≈ 1.6 $\mu\Omega$ cm and the residual resistivity ratio RRR ≈ 11 , the critical current density at zero magnetic field is $J_{c0} \approx 4 \times 10^5$ A/cm², and $\mu_0 H_{c2}(5$ K) ≈ 15 T; the anisotropy factor of the upper critical field at $T = 5$ K is $\gamma \approx 4.4$ [13,14].

Sample P6 has a nearly parallelepiped shape with $w \approx 1.1$ mm, $t \approx 0.8$ mm and $h \approx 1.4$ mm. The main characteristic parameters of sample P6 are: $T_c^{onset} \approx 9.1$ K, $\Delta T_c \approx 0.3$ K, RRR ≈ 1.1 , $\rho(40$ K) ≈ 130 $\mu\Omega$ cm. The critical current density at $T = 5$ K and at zero magnetic field is $J_{c0} \approx 3 \times 10^4$ A/cm²; it exhibits a monotonic decrease with the magnetic field, following roughly an exponential law. The upper critical field is isotropic and its value at $T = 5$ K is $\mu_0 H_{c2} \approx 2$ T.

The effects of the neutron irradiation on both superconducting and normal-state properties of a large series of Mg¹¹B₂ bulk samples, including sample P0 and P6, have extensively been investigated in Refs. [13,14,17]. On increasing the neutron fluence, it has been observed a monotonic decrease of T_c and an increase of the residual normal-state resistivity $\rho(T_c)$. Nevertheless, it has been shown that the irradiation does not affect the variation of the normal-state resistivity $\Delta\rho = \rho(300\text{ K}) - \rho(T_c)$. As suggested by Rowell [41], just $\Delta\rho$ is a parameter that gives information on the grain connectivity. The results reported in Ref. [13] show that $\Delta\rho$ remains of the order of $10\ \mu\Omega\text{ cm}$ over the whole range of irradiation level; in particular, in sample P0 $\Delta\rho = 16\ \mu\Omega\text{ cm}$ and in sample P6 $\Delta\rho = 12\ \mu\Omega\text{ cm}$, indicating that thermal-neutron irradiation does not affect the grain-boundary properties. On the other hand, it has been shown that either neutron irradiation or He-ion irradiation [11] do not affect the grain connectivity, even at high irradiation levels, contrary to what occurs using heavy-ion irradiation [12]. Recent studies by transmission electron microscopy have highlighted that neutron irradiation in these samples creates nanometric amorphous regions (mean diameter $\sim 4\text{ nm}$) in the crystal lattice, whose density scales with the neutron dose [17]. Studies on the field dependence of the critical current density have shown that at moderate neutron-fluence levels ($\leq 10^{19}\text{ cm}^{-2}$) such defects introduce new pinning centers, leading to an improvement of the critical current density; on the contrary, for neutron fluence higher than 10^{19} cm^{-2} (as for sample P6) these nanometric defects do not act as pinning centers because they are smaller than the coherence length [17]. Moreover, these studies have shown that in the pristine and the heavily irradiated samples the pinning mechanism is ruled by grain boundaries. The defects induced by neutron irradiation act as inter- and intra-band scattering centers; the intra-band scattering causes a reduction of the electron mean free path and is responsible for the growth of the normal-state resistivity. The reduction of T_c has been ascribed to both the scattering processes and the smearing of the electron density of states near the Fermi surface [11,13].

Although in the two samples ΔT_c is roughly the same, in sample P6, due to the reduced T_c value, $\Delta T_c/T_c \approx 0.03$, affecting noticeably the temperature dependence of the mw surface resistance near T_c . On the other hand, from AC susceptibility measurements at 100 kHz, we have found that the first derivative of the real part of the AC susceptibility can be described by a Gaussian distribution function of T_c , centered at $T_{c0} = 8.5 \pm 0.1\text{ K}$ with $\sigma_{T_c} = 0.2 \pm 0.05\text{ K}$. In the following, we will use this distribution function to quantitatively discuss the results obtained in sample P6. On the contrary, for sample P0, $\Delta T_c/T_c$ is one order of magnitude smaller, not noticeably affecting the $R_s(T)$ curve.

The mw surface resistance has been measured using the cavity-perturbation technique [27]. A copper cavity, of cylindrical shape with golden-plated walls, is tuned in the TE₀₁₁ mode resonating at $\omega/2\pi \approx 9.6\text{ GHz}$. The sample is located in the center of the cavity, by a sapphire

rod, where the mw magnetic field is maximum. The cavity is placed between the poles of an electromagnet which generates DC magnetic fields up to $\mu_0 H_0 \approx 1\text{ T}$. Two additional coils, independently fed, allow compensating the residual field and working at low magnetic fields. A liquid-helium cryostat and a temperature controller allow working either at fixed temperatures or at temperature varying with a constant rate. The sample and the field geometries are shown in Fig. 1a; the DC magnetic field is perpendicular to the mw magnetic field, \mathbf{H}_ω . When the sample is in the mixed state, the induced mw current causes a tilt motion of the whole vortex lattice [31]; Fig. 1b schematically shows the motion of a flux line.

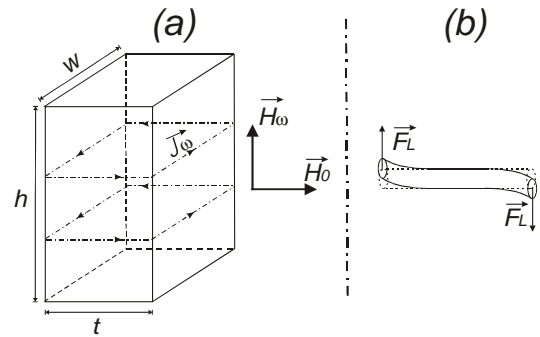


Fig. 1. (a) Field and current geometry at the sample surface. (b) Schematic representation of the motion of a flux line.

The surface resistance of the sample is given by

$$R_s = \Gamma \left(\frac{1}{Q_L} - \frac{1}{Q_U} \right),$$

where Q_L is the quality factor of the cavity loaded with the sample, Q_U that of the empty cavity and Γ the geometry factor of the sample.

The quality factor of the cavity has been measured by an hp-8719D Network Analyzer. The surface resistance has been measured as a function of the temperature, at fixed values of the DC magnetic field, and as a function of the field, at fixed temperatures. All the measurements have been performed at very low input power; the estimated amplitude of the mw magnetic field in the region in which the sample is located is of the order of $0.1\ \mu\text{T}$.

3 Experimental results

Figure 2 shows the temperature dependence of the surface resistance in the pristine (a) and irradiated (b) MgB₂ samples, at different values of the DC magnetic field. In order to disregard the geometry factor, and compare the results in samples of different dimensions, we have normalized the data to the value of the surface resistance in the normal state, R_n , at $T = T_c^{onset}$. The results have been obtained according to the following procedure: the sample was zero-field cooled (ZFC) down to low temperature,

then H_0 was set at a given value and kept constant during the time the measurement has been performed.

On increasing H_0 , the $R_s(T)$ curves broaden and shift towards lower temperatures; however, the effects of the applied magnetic field is different in the two samples. Although the value of H_{c2} of sample P0 at low temperatures is one order of magnitude larger than that of P6, the field-induced variations of R_s in the two samples have roughly the same magnitude. In sample P0, one can observe an anomalously enhanced field-induced broadening of the $R_s(T)$ curve, which extends down to the lowest temperature. On the contrary, in sample P6 the larger shift of the $R_s(T)$ curve induced by H_0 is expected because of the lower H_{c2} value.

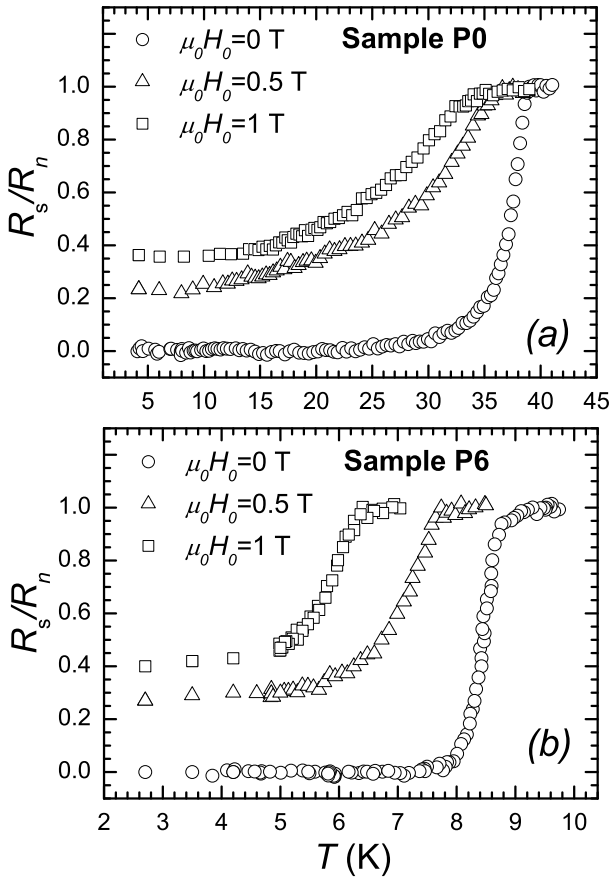


Fig. 2. Normalized values of the surface resistance as a function of the temperature, obtained in the two samples, at different values of the DC field. R_n is the surface resistance at $T = T_c$.

The field-induced variations of R_s have been investigated for different values of the temperature. For each measurement, the sample was ZFC down to the desired temperature; the DC magnetic field was increased up to a certain value and, successively, decreased down to zero. Figures 3, 4 and 5 show the field-induced variations of R_s for the two samples, at different temperatures. In all the figures, $\Delta R_s(H_0) \equiv R_s(H_0, T) - R_{res}$, where R_{res} is the residual mw surface resistance at $T = 2.5$ K and $H_0 = 0$;

moreover, the data are normalized to the maximum variation, $\Delta R_s^{max} \equiv R_n - R_{res}$. The continuous lines reported in the figures are the best-fit curves obtained by the model reported in Sec. 4.

In both samples, R_s does not show any variation as long as the magnetic field reaches a certain value, depending on T , that identifies the first-penetration field, H_p . For $H_0 > H_p$, vortices start to penetrate the sample and, consequently, R_s increases.

Figure 3 refers to the results obtained at $T = 4.2$ K. At this temperature, in both samples the $R_s(H_0)$ curves exhibit a magnetic hysteresis, which disappears for H_0 higher than a certain value, indicated in the figure as H' . The inset in panel (b) shows a minor hysteresis loop obtained by sweeping H_0 from 0 to 0.25 T and back. The field-induced variations of R_s in sample P0 show some anomalies. Firstly, the application of a magnetic field of ≈ 1 T, which is about $H_{c2}/15$, causes a R_s variation of $\approx 35\%$ of the maximum variation. These field-induced variations of R_s are much greater than those expected from the models reported in the literature [30,31,32] and detected in other superconductors [28,29]. A comparison with the results of panel (b) shows that in sample P6 a R_s variation of the same order is obtained for the same value of H_0 , even though, in this case, 1 T is about $H_{c2}/2$. Results similar to those obtained in P0 have been observed in other MgB₂ samples, produced by different methods and, therefore, seems to be a peculiarity of MgB₂ [35,37,38,40]. The finding that in sample P6 we have not observed this anomalous result strongly suggests that the enhanced R_s variation is due to the two-gap superconductivity.

A magnetic hysteresis of R_s is expected in superconducting samples in the critical state; it is ascribable to the different magnetic induction at increasing and decreasing DC fields [42]. Most likely, the different amplitude of the hysteresis loop obtained in the two samples is due to the different values of the critical current density; a smaller hysteresis is observed in sample P6 because of the smaller J_c value. However, as it is visible in Fig. 3, also the shape of the hysteresis loop is different in the two samples. The decreasing-field branch of the $R_s(H_0)$ curve in sample P6 has a negative concavity down to H_p , as expected [42]. On the contrary, in sample P0 one can observe a plateau, in the field range $0 \div 0.2$ T, which cannot be justified in the framework of the critical-state models, considering the measured field dependence of J_c [13]. We would like to remark that this result has been obtained in all of the MgB₂ samples we have investigated [38,40].

Figure 4 shows the field-induced variations of R_s , for sample P0 (a), at $T = 30$ K, and for sample P6 (b), at $T = 7$ K; for both samples, $T/T_c \approx 0.77$. In the $R_s(H_0)$ curve of sample P0 the hysteresis is still present, probably due to the high value of J_c at this temperature, and still has an anomalous shape. We remark that in sample P0 we have observed magnetic hysteresis of R_s up to $T/T_c \approx 0.95$, while in sample P6 the hysteresis becomes undetectable at $T/T_c \gtrsim 0.55$.

Figure 5 shows the field-induced variations of R_s at temperatures near T_c , where in both samples the $R_s(H_0)$

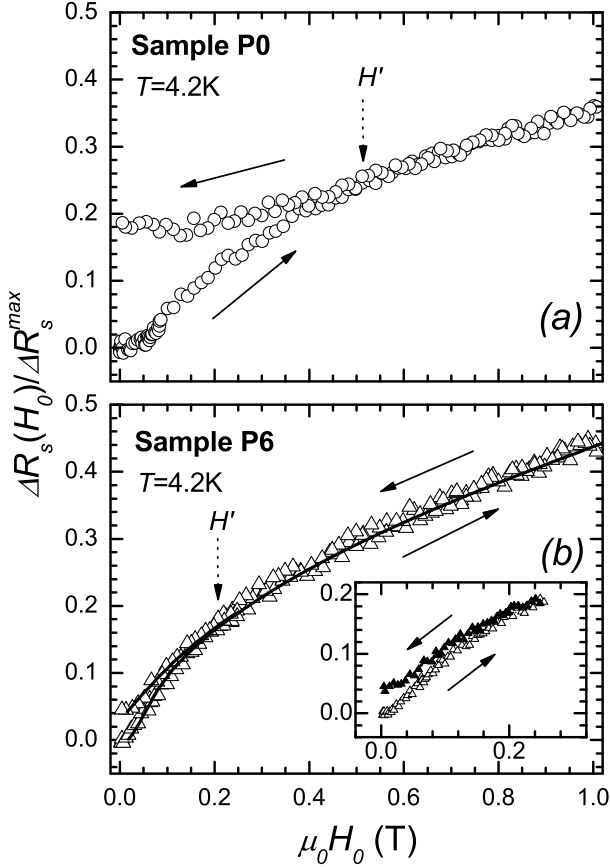


Fig. 3. Field-induced variations of R_s for samples P0 (a) and P6 (b), at $T = 4.2$ K. $\Delta R_s(H_0) \equiv R_s(H_0, T) - R_{res}$, where R_{res} is the residual mw surface resistance at $T = 2.5$ K and $H_0 = 0$; $\Delta R_s^{\max} \equiv R_n - R_{res}$. The line is the best-fit curve obtained, as explained in Sec. 5, with $\mu_0 H_{c2} = 1.71$ T, $\omega_0/\omega = 0.67$ and the field dependence of the critical current density reported in Ref. [13]. The inset shows a minor hysteresis loop obtained by sweeping H_0 from 0 to 0.25 T and back.

curve is reversible. As will be shown in Sec. 5, at temperatures near T_c the field dependence of the mw surface resistance can be accounted for by standard models also for sample P0, provided that the anisotropy of the upper critical field is taken into account.

From isothermal $R_s(H_0)$ curves, obtained at different temperatures, we have deduced the temperature dependence of the characteristic fields, H_p , H_{c2} and H' . In Fig. 6 we report the values of H_p , H_{c2} and H' as a function of the reduced temperature, T/T_c^{onset} , for the two samples. The inset in panel (b) shows $H_{c2}(T)$ of sample P6 in an enlarged scale.

From Fig. 6a, one can see that H_p of sample P0 exhibits a linear temperature dependence down to low temperatures, consistently with results reported by different authors in bulk [43, 44] and crystalline [45, 46] MgB₂ samples. The extrapolated value at $T = 0$ is about 55 mT; so, considering the demagnetization effect, the estimated value of the lower critical field is $H_{c1}(0) \approx 70$ mT. This value, although consistent with the lower critical field reported for MgB₂ crystals by some authors [46], is slightly

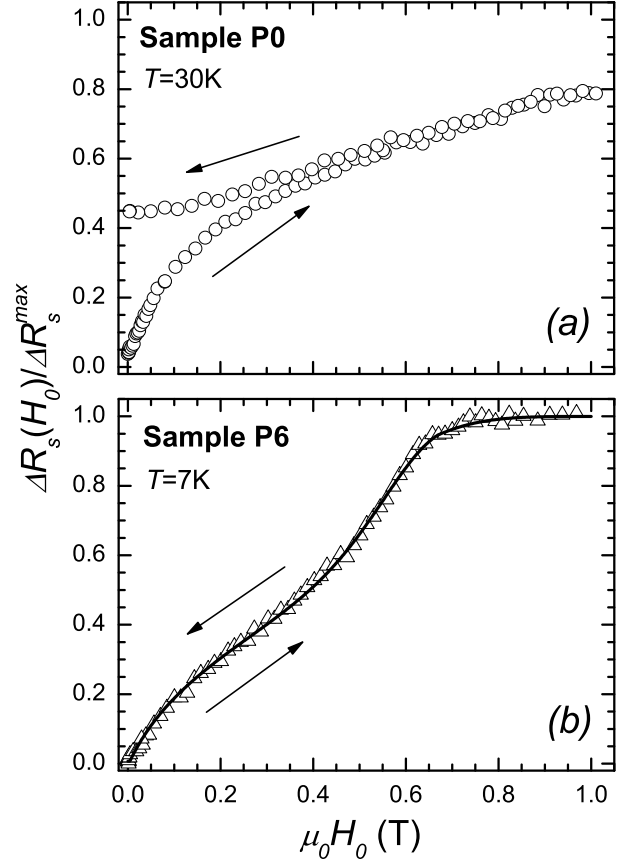


Fig. 4. Normalized field-induced variations of R_s for samples P0 (a) and P6 (b), at $T/T_c \approx 0.77$. The line in panel (b) is the best-fit curve of the data, obtained as described in the text by using the field dependence of the depinning frequency reported in Fig. 9.

larger than that reported for bulk samples, which ranges from 15 to 45 mT. We suggest that this is ascribable to weak surface-barrier effects.

In sample P6 we have obtained H_p values smaller, but of the same order, than those of sample P0; this may be due to the irradiation effects. Indeed, the authors of Ref. [18], from magnetization measurements in neutron-irradiated MgB₂ crystals, have observed that the lower critical field reduces monotonically on increasing the fluence.

The values of $H_{c2}(T)$ indicated in Fig. 6b as open triangles have been deduced measuring the magnetic field at which R_s reaches the normal state value, R_n . At temperatures in which the upper critical field of sample P6 is higher than the maximum magnetic field achievable with our experimental apparatus (≈ 1 T), the $H_{c2}(T)$ values (full triangles in the figure) have been obtained as best-fit parameters, using the model reported in Sec. 4. On the contrary, since the results obtained in sample P0 cannot be accounted for by the model (except at temperature close to T_c), we report only the values we have directly deduced from the experimental results. For $T \geq 5$ K, the values we obtained for $H_{c2}(T)$, in both samples, agree with those reported in Ref. [13] (the authors do not report H_{c2} at lower

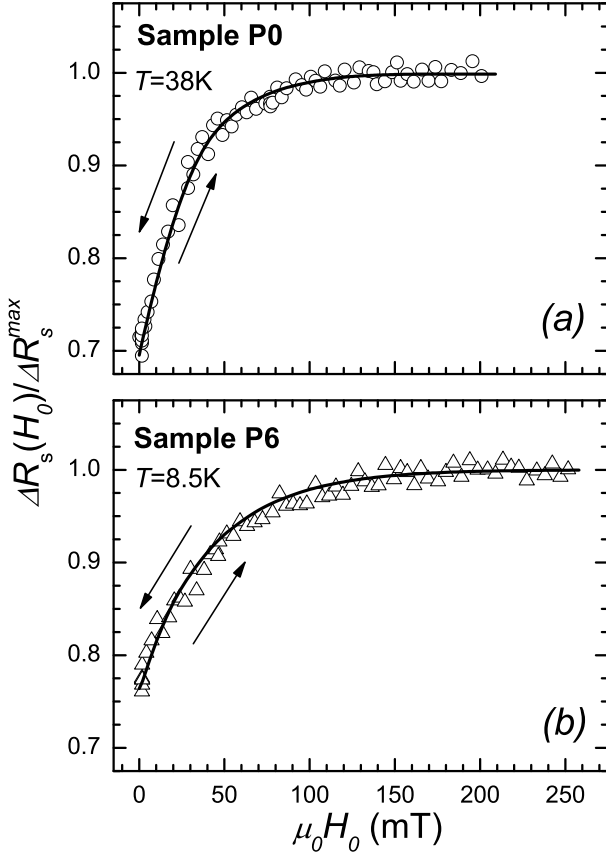


Fig. 5. Normalized field-induced variations of R_s for samples P0 (a) and P6 (b), at temperatures close to T_c . Lines are best-fit curves, obtained by the model of Sec. 4 considering fluxons move in the flux-flow regime. The line of panel (a) has been obtained taking into account the anisotropy of the upper critical field, as described in the text, with $\gamma = 3.3$; for sample P0, we have set $\gamma = 1$ consistently with the results of Ref. [14].

temperatures). Our results give complementary information about the temperature dependence of H_{c2} of sample P6 at low temperatures. The continuous line in Fig. 6b has been obtained by fitting the data of sample P6 with $H_{c2}(T) = H_{c20}[1 - (T/T_c)^\alpha]$; we have obtained, as best-fit parameters, $\mu_0 H_{c20} = (2.2 \pm 0.2)$ T, $\alpha = 1.9 \pm 0.3$ and $T_c = (8.9 \pm 0.2)$ K. This temperature dependence of the upper critical field is consistent with that expected in conventional superconductors. On the contrary, for sample P0 we observed an upward curvature of $H_{c2}(T)$, clearly visible in the inset, characteristic of two-gap MgB₂ materials [1, 4, 5].

$H'(T)$ of Fig. 6c corresponds to the value of the DC magnetic field at which the decreasing-field branch of the $R_s(H_0)$ curves deviates from the increasing-field branch. The zero values (without error bar) mean that the hysteresis is not detectable at the corresponding temperatures. Consistently with the lower value of the critical current density, $H'(T)$ is smaller in sample P6 than in P0. We would like to remark that the values of $H'(T)$ could differ from the irreversibility field deduced from magnetization measurements. Indeed, it has been shown that, in sam-

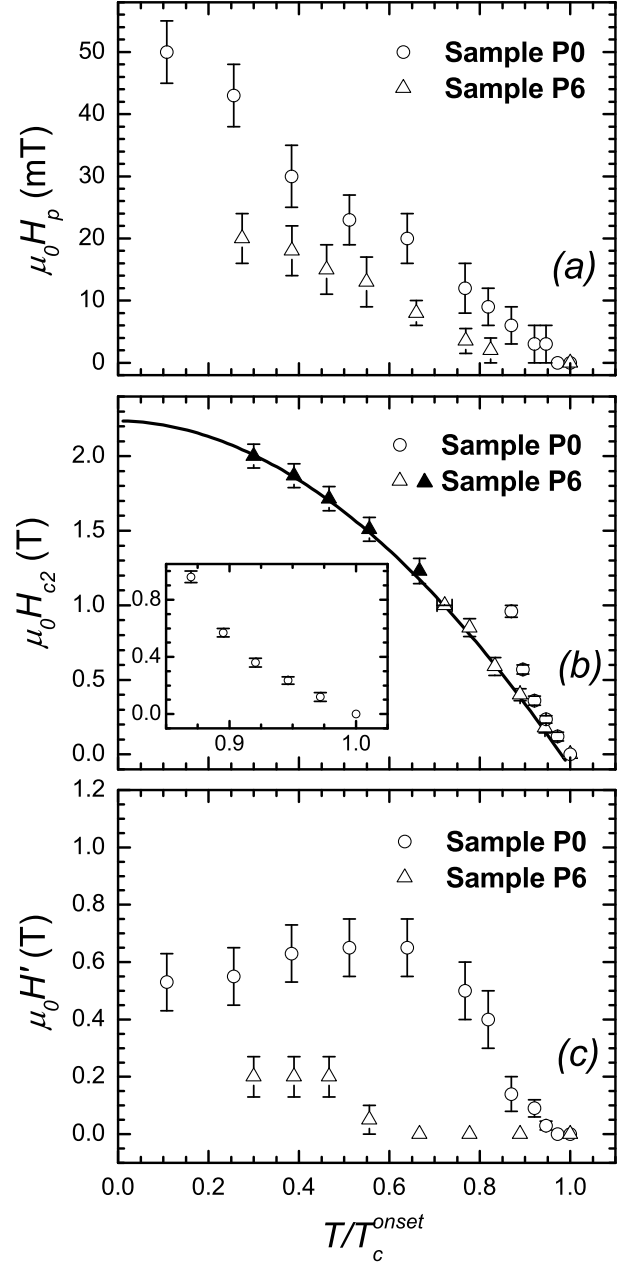


Fig. 6. Temperature dependence of the characteristic fields, H_p , H_{c2} and H' , for the two samples. In panel (b): the inset shows the $H_{c2}(T)$ values of sample P6 in an enlarged scale; the continuous line is the best-fit curve of the experimental data, obtained for sample P6, as described in the text.

ples of finite dimensions, the application of an AC magnetic field normal to the DC field can induce the fluxon lattice to relax toward an uniform distribution [47]. Furthermore, measurements we have performed in different superconducting samples have pointed out that, for samples of millimetric size, the sensitivity of our experimental apparatus does not allow resolving magnetic hysteresis of R_s when $J_c < 10^4$ A/cm². By considering the values of J_c reported in Ref. [13], at $T = 4.2$ K we should obtain $\mu_0 H' \approx 0.2$ T for sample P6 and $\mu_0 H' \approx 3.5$ T for sam-

ple P0. From Fig. 6c, one can see that this expectation is verified in sample P6; on the contrary, the value of H' in sample P0 is about one order of magnitude smaller than the expected one.

4 The model

Microwave losses induced by static magnetic fields have been investigated by several authors [27, 28, 29, 30, 31, 32, 42, 48]. At low temperatures and for applied magnetic fields lower enough than the upper critical field, the main contribution arises from the fluxon motion; however, it has been pointed out that a noticeable contribution can arise from the presence of normal fluid, especially at temperatures near T_c and for magnetic fields of the same order of $H_{c2}(T)$. The majority of the models assume a uniform distribution of fluxons inside the sample; so, they disregard the effects of the critical state. Very recently, we have investigated the field-induced variations of the mw surface resistance in superconductors in the critical state [42, 48], and have accounted for the magnetic hysteresis in the $R_s(H_0)$ curves.

In the London local limit, the surface resistance is proportional to the imaginary part of the complex penetration depth, $\tilde{\lambda}$, of the em field:

$$R_s = -\mu_0\omega \operatorname{Im}[\tilde{\lambda}(\omega, B, T)]. \quad (1)$$

The complex penetration depth has been calculated in different approximations [30, 31]. Coffey and Clem (CC) have elaborated a comprehensive theory for the electromagnetic response of superconductors in the mixed state, in the framework of the two-fluid model of superconductivity [30]. The theory has been developed under two basic assumptions: i) inter-vortex spacing much less than the field penetration depth; ii) uniform vortex distribution in the sample. With these assumptions vortices generate a magnetic induction field, B , uniform in the sample. This approximation is valid for $H_0 > 2H_{c1}$ whenever the fluxon distribution can be considered uniform within the AC penetration depth.

In the linear approximation, $H_\omega \ll H_0$, $\tilde{\lambda}(\omega, B, T)$ expected from the CC model is given by

$$\tilde{\lambda}(\omega, B, T) = \sqrt{\frac{\lambda^2(B, T) + (i/2)\tilde{\delta}_v^2(\omega, B, T)}{1 - 2i\lambda^2(B, T)/\delta_{nf}^2(\omega, B, T)}}, \quad (2)$$

with

$$\lambda(B, T) = \frac{\lambda_0}{\sqrt{[1 - w_0(T)][1 - B/B_{c2}(T)]}}, \quad (3)$$

$$\delta_{nf}(\omega, B, T) = \frac{\delta_0(\omega)}{\sqrt{1 - [1 - w_0(T)][1 - B/B_{c2}(T)]}}, \quad (4)$$

where λ_0 is the London penetration depth at $T = 0$, δ_0 is the normal-fluid skin depth at $T = T_c$, $w_0(T)$ is the fraction of normal electrons at $H_0 = 0$; in the Gorter and Casimir two-fluid model $w_0(T) = (T/T_c)^4$.

$\tilde{\delta}_v$ is the effective complex skin depth arising from the vortex motion; it depends on the relative magnitude of the viscous and restoring-pinning forces, which identifies the depinning frequency ω_0 . $\tilde{\delta}_v$ can be written as

$$\frac{1}{\tilde{\delta}_v^2} = \frac{1}{\delta_f^2} \left(1 + i \frac{\omega_0}{\omega}\right), \quad (5)$$

where

$$\delta_f^2 = \frac{2B\phi_0}{\mu_0\omega\eta}, \quad (6)$$

with η the viscous-drag coefficient and ϕ_0 the quantum of flux.

When the frequency of the em wave, ω , is much lower than ω_0 , the fluxon motion is ruled by the restoring-pinning force. On the contrary, for $\omega \gg \omega_0$, the fluxon motion takes place around the minimum of the pinning-potential well and, consequently, the restoring-pinning force is nearly ineffective. So, the contribution of the viscous-drag force predominates and the induced em current makes fluxons move in the flux-flow regime. In this case, enhanced field-induced energy losses are expected.

As it is clear from Eqs. (1–4), it is expected that the features of the $R_s(H_0)$ curves strongly depend on the applied-field dependence of B . On the other hand, the CC theory is strictly valid when B is uniform inside the sample; in particular for $H_0 \gg H_{c1}$, the $R_s(H_0)$ curves can be described setting $B = \mu_0 H_0$. When fluxons are in the critical state, the assumption of uniform B is no longer valid and the CC theory does not correctly describe the field-induced variations of R_s . As a consequence, the hysteresis in the $R_s(H_0)$ curve cannot be justified by Eqs. (1–4). In our field geometry (see Fig. 1a), the effects of the non-uniform B distribution on R_s are particularly enhanced because in the two surfaces of the sample normal to the external magnetic field the mw current and fields penetrate along the fluxon axis and, consequently, the mw losses involve the whole vortex lattice. However, in this case, one can easily take into account the non-uniform B distribution by calculating a proper averaged value of R_s over the whole sample as follows [42, 48]

$$R_s = \frac{1}{S} \int_{\Sigma} R_s(|B(\mathbf{r})|) dS, \quad (7)$$

where Σ is the sample surface, S is its area and \mathbf{r} identifies the surface element.

The pinning effects are particularly enhanced at temperatures smaller enough than T_c , where the dissipations are essentially due to vortex motion. So, the main contribution to R_s comes from the sample regions in which fluxons experience the Lorentz force due to the mw current, i.e. where $\mathbf{H}_0 \times \mathbf{J}_\omega \neq 0$. Furthermore, in order to take into due account the critical-state effects by Eq. (7), it is essential to know the B profile inside the sample, determined by $J_c(B)$.

Recently, using this method, we have investigated the effects of the critical state on the field-induced variation of R_s , at increasing and decreasing fields [42, 48]. We have shown that the parameter that mainly determines the peculiarities of the $R_s(H_0)$ curve is the full penetration field,

H^* . Firstly, the width of the hysteresis is directly related to the value of H^* ; samples of small size and/or small J_c are expected to exhibit weak hysteretic behavior. Furthermore, H^* determines the shape of the hysteresis loop as well. On increasing the external field from zero up to H^* , more and more sample regions contribute to the mw losses; this gives rise to a positive curvature of the increasing-field branch of the $R_s(H_0)$ curve. For $H_0 > H^*$, in the whole sample the local magnetic induction depends about linearly on the external field and the increasing-field branch is expected to have a negative concavity. The shape of the decreasing-field branch is strictly related to the shape of the magnetization curve; it should exhibit a negative concavity, with a monotonic reduction of R_s in the whole field range swept.

5 Discussion

As we have shown in Sec. 3, the $R_s(H_0, T)$ curves exhibit different peculiarities in the unirradiated sample (P0) and the strongly irradiated sample (P6). The model described in Sec. 4 fully justifies the experimental results obtained in sample P6, which exhibits a single-gap superconductivity [15,16]. On the contrary, the results obtained in sample P0 cannot be justified in the framework of the same model, either for the magnetic-field dependence or for the temperature dependence of the surface resistance, even at zero DC field. Only the results obtained at temperatures close to T_c can be justified, provided that the anisotropy of the upper critical field is taken into due account. In the following, firstly we will discuss the temperature dependence of the mw surface resistance in the absence of DC magnetic fields; successively, we will discuss the field-induced variations of R_s .

5.1 Temperature dependence of R_s in zero magnetic field

Figure 7 shows the normalized values of the surface resistance at $H_0 = 0$ as a function of the reduced temperature for both samples. The $R_s(T)$ curve of sample P6 shows a wide transition, broadened in a roughly symmetric way with respect to the middle point at $R_s/R_n = 0.5$. This behavior can be ascribed to the T_c distribution over the sample. On the contrary, in sample P0 one can notice a sharp variation of $R_s(T)$, at temperatures near T_c , and a wide tail, extending from $T/T_c \approx 0.9$ down to $T/T_c \approx 0.7$, which cannot be ascribed to the T_c distribution. The lines in the figure are best-fit curves; they have been obtained with different procedures for the two samples.

The results obtained from the model discussed in Sec. 4 setting $B = 0$ in Eqs. (1–4) converge to those of the em response of superconductors in the Meissner state, in the framework of the two-fluid model. In this case, the temperature dependence of R_s/R_n is determined, apart from the T_c distribution over the sample, by the temperature dependence of the normal-fluid density, $w_0(T)$, and the ratio λ_0/δ_0 . In order to fit the experimental data obtained

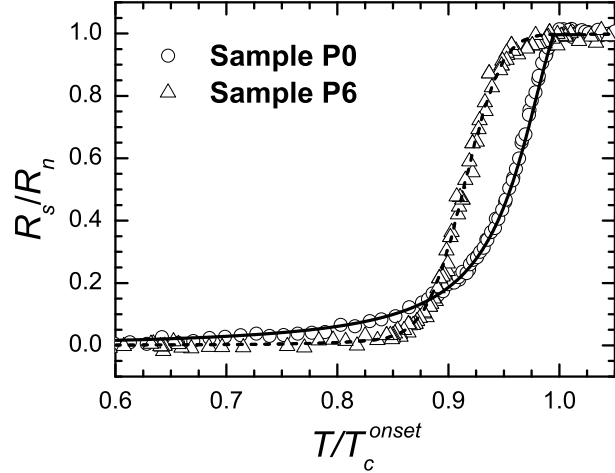


Fig. 7. Normalized values of the mw surface resistance as a function of the reduced temperature, obtained in the two samples at $H_0 = 0$. Symbols are experimental data; lines are the best-fit curves obtained as described in the text.

in sample P6, we have assumed $w_0(T) = (T/T_c)^4$, consistently with the Gorter and Casimir two-fluid model, and have used Eqs. (1–4) with $B = 0$. We have averaged the expected curve over a gaussian distribution function of T_c with $T_{c0} = 8.5$ K and $\sigma = 0.2$ K (see Sec. 2) and have used λ_0/δ_0 as fitting parameter. The best-fit curve, dashed line in Fig. 7, has been obtained with $\lambda_0/\delta_0 = 0.14$; however, we have found that the expected curve is little sensitive to variations of λ_0/δ_0 , except at low temperatures, where the measured R_s is limited by the sensitivity of our experimental apparatus. In particular, by varying T_{c0} and σ within the experimental uncertainty, good agreement is obtained with λ_0/δ_0 values ranging from 0.04 to 0.15. This occurs because the T_c distribution broadens the $R_s(T)$ curve, hiding the λ_0/δ_0 effects.

Unlike for sample P6, the results of Fig. 7 obtained in P0 cannot be justified in the framework of the Gorter and Casimir two-fluid model, using reasonable values of λ_0/δ_0 . On the other hand, different authors [2,6,49] have shown that the temperature dependence of the field penetration depth in MgB₂ cannot be accounted for by either the Gorter and Casimir two-fluid model or the standard BCS theory. A linear temperature dependence of the condensed fluid density, in a wide range of temperatures below T_c , has been reported, which has been justified in the framework of two-gap models for the MgB₂ superconductor [6,49]. Prompted by these considerations, we have hypothesized a linear temperature dependence of w_0 . The continuous line in Fig. 7 is the best-fit curve; it has been obtained by Eqs. (1–4) with $B = 0$, $w_0(T) = T/T_c$ and $\lambda_0/\delta_0 = 0.15$. The wide low- T tail is essentially determined by the linear temperature dependence of w_0 . The sensitivity achievable by our experimental apparatus does not allow determining the small variations of $R_s(T)$ for $T/T_c \lesssim 0.5$; so, from $R_s(T)$ measurements no indication about the temperature dependence of the densities of the normal and condensed fluids at low temperatures can be

obtained. However, the linear temperature dependence of the lower critical field we obtained (see Fig. 6a) strongly suggests that w_0 linearly depends on T down to low temperatures.

5.2 Field dependence of R_s in sample P6

In conventional (single-gap) superconductors, it is expected that the field dependence of the mw surface impedance is described by the model reported in Sec. 4. In this framework, in order to calculate the expected field-induced variations, by Eqs. (1–4), the essential parameters are the value of λ_0/δ_0 , $H_{c2}(T)$, the depinning frequency, ω_0 , and its field dependence. It is not necessary to consider the upper-critical-field anisotropy, γ , because it has been shown that in the P6 sample $\gamma = 1$ [14]. When the critical-state effects cannot be neglected, in order to use Eq. (7), it is also essential to know the profile of the induction field determined by the field dependence of the critical current density. The value of λ_0/δ_0 has been determined by fitting the $R_s(T)$ curve at $H_0 = 0$; the critical current density and its field dependence are reported in Ref. [13]. The values of $H_{c2}(T)$ at $T \geq 5$ K are reported in Ref. [13], and/or deduced from our experimental data; at $T < 5$ K, H_{c2} has to be considered as parameter. It is worth noting that the large uncertainty of λ_0/δ_0 , we obtained for this sample, does not affect the best-fit curves because this parameter essentially determines the normalized $\Delta R_s(H_0)$ value at $B = 0$.

As one can see from Fig. 3, at $T = 4.2$ K the $R_s(H_0)$ curve exhibits a magnetic hysteresis, indicating that the effects of the critical state are not negligible. In order to use Eq. (7), we have calculated the B profile in the sample using the field dependence of the critical current, $J_c(B)$, reported in Ref. [13] and we have set the induction field at the edges of the sample as $B = \mu_0(H_0 - H_p)$; we have taken H_{c2} and ω_0 as fitting parameters. The line of Fig. 3b is the best-fit curve; it has been obtained with $\mu_0 H_{c2} = 1.71$ T and $\omega_0/\omega = 0.67$ independent of H_0 . For the sake of clarity, in Fig. 8 we report the results obtained by sweeping the DC magnetic field from 0 to 0.25 T and back, along with the expected curve. The inset shows the B profile along the width of the sample at half height, determined by $J_c(B)$; the continuous lines are the increasing-field profiles, the dashed ones are the decreasing-field profiles at the same external-field values. As one can see, taking into account the field distribution inside the sample, the experimental results are quite well justified in the framework of the model discussed in Sec. 4. In the increasing-field branch, a change of concavity is well visible at $\mu_0(H_0 - H_p) \approx 0.04$ T, consistently with the expected value of the full penetration field; the decreasing-field branch exhibits a negative concavity in the whole range of fields.

Following the procedure above described, from the best fit of the experimental data of the isothermal $R_s(H_0)$ curves at $T < 6$ K we have obtained the $H_{c2}(T)$ values indicated as full triangles in Fig. 6b.

When the $R_s(H_0)$ curves do not show hysteresis, the effects of the critical state are negligible and the induction

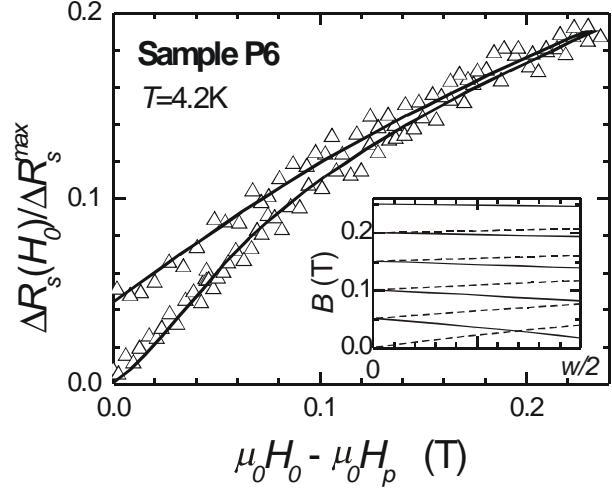


Fig. 8. Field-induced variations of the mw resistance, obtained in sample P6 by sweeping the magnetic field from 0 to 0.25 T and back. The line is the best-fit curve obtained, as explained in the text, with $\mu_0 H_{c2} = 1.71$ T, $\omega_0/\omega = 0.67$ and the field dependence of the critical current density reported in Ref. [13]. The inset shows the B profile at increasing (—) and decreasing (- -) fields; w is the width of the sample.

field, B , can be considered uniform. In this case, we have used the following approximate expression for the magnetization:

$$M = -H_p + \frac{H_p}{H_{c2} - H_p}(H_0 - H_p);$$

and, consequently

$$B = \mu_0 \left(1 + \frac{H_p}{H_{c2} - H_p} \right) (H_0 - H_p).$$

Several calculations have shown that, in order to fit the experimental data at $T \geq 7$ K, it is essential to consider the T_c distribution over the sample. So, we have averaged the expected $R_s(H_0)$ curves [calculated by Eqs. (1–4)] over the T_c distribution (see Sec. 2). We have used for $H_p(T)$ and $H_{c2}(T)$ the values deduced from the experimental data, letting them vary within the experimental uncertainty, and have considered the depinning frequency as parameter. The lines of Figs. 4 and 5 have been obtained by this procedure.

By fitting the results at $T = 7$ K, we have obtained the field dependence of ω_0/ω reported in Fig. 9. The roughly constant value of ω_0/ω we obtained up to $\mu_0 H_0 \approx 0.3$ T indicates that in this field range individual vortex pinning occurs; on further increasing the magnetic field, the interaction between fluxons becomes important, collective vortex pinning sets in and, consequently, the depinning frequency decreases. The data obtained at $\mu_0 H_0 \gtrsim 0.65$ T are well fitted setting $\omega_0/\omega = 0$ in Eq. (5); this means that, at $T = 7$ K and $\mu_0 H_0 \gtrsim 0.65$ T, the induced mw current makes fluxons move in the flux-flow regime.

The best-fit curve of Fig. 5 has been obtained with $\omega_0/\omega = 0$, as expected. Indeed, at temperature very close

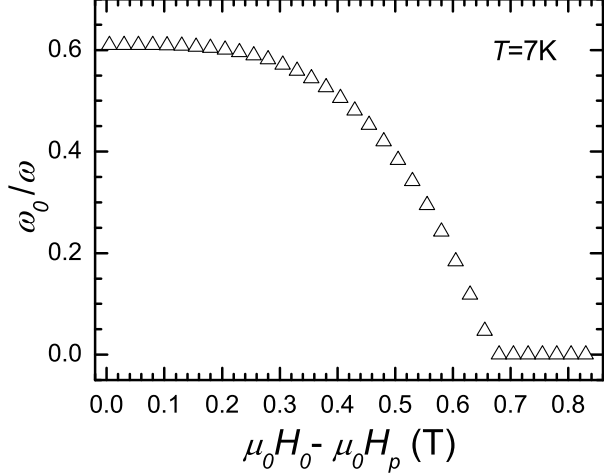


Fig. 9. Magnetic field dependence of the depinning frequency, obtained for sample P6 by fitting the experimental results reported in Fig. 4b.

to T_c , the pinning effects are weak and the induced mw current makes fluxons move in the flux-flow regime.

5.3 Field dependence of R_s in sample P0

It has been shown by several authors that the properties of the two-gap MgB₂ superconductor in the mixed state cannot be accounted for by standard theories [1, 3, 18, 19, 20, 35, 36, 39]. It is by now accepted that this is related to the double-gap nature of MgB₂ that is responsible for an unusual vortex structure. Indeed, it has been highlighted, both experimentally and theoretically, that the vortex cores are characterized by two different spatial and magnetic-field scales [21, 22]. Because of the different magnetic-field dependence of the two gaps, on varying the field, the structure of the vortex lattice changes in an unusual way. At low magnetic fields, quasiparticles by π and σ bands are trapped within the vortex core, even if on different spatial scales because of the different coherence lengths ξ_π and ξ_σ ; in the field range 0.5 ÷ 1 T, though σ -band quasiparticles remain localized, the π -band quasiparticles spread over the sample [22]; on further increasing the field, Δ_π is strongly reduced, the π -quasiparticle contribution remains almost unchanged while the σ -quasiparticle contribution continues to increase with about the same rate up to the macroscopic H_{c2} . So, a further characteristic field is needed for determining the fluxon-lattice properties of MgB₂; the existence of this crossover field, often indicated as H_{c2}^π , has been highlighted in several experiments [1, 3, 22, 23, 24, 25]. The field-induced evolution of the vortex lattice is expected to affect the vortex-vortex and vortex-pinning interactions, making the standard models most likely inadequate to describe the fluxon dynamics.

Results on the field-induced variations of R_s in MgB₂ have been reported by some authors [35, 36, 37, 38, 39, 40, 50]; most of them have highlighted several anomalies, which

cannot be explained in the framework of standard models for fluxon dynamics. In particular, it has been highlighted unusually enhanced field-induced mw losses at applied magnetic field much lower than H_{c2} . Only Zaitsev et al. [50] have explained the frequency and field dependence of the mw surface resistance of MgB₂ films in the framework of standard models. The results we have obtained in sample P0 are similar to those reported by Shibata et al. [35], who investigated the field dependence of the surface impedance in MgB₂ single crystal in a wide range of DC magnetic fields (up to 14 T). At low temperatures, the authors have observed an initial fast variation of the field-induced mw dissipation up to fields of the order of 1 T, followed by a slower one at higher fields. Consistently with the sharp field-induced variation of the heat capacity and thermal conductivity, the enhanced low-field variation of the mw losses has been ascribed to the high increase of π quasiparticles in the vortex cores. At higher fields, the variation is slower because of the saturation of the π -quasiparticle contribution.

According to Shibata et al., the enhanced field-induced variation we observed in sample P0 can be qualitatively ascribed to the strong reduction of Δ_π in the field range we have investigated. However, the observed $R_s(H_0)$ curves differ from the expected ones in both the intensity and the shape. Here, we discuss the shape of the $R_s(H_0)$ curves.

In a wide range of temperatures below T_c , we have observed a magnetic hysteresis, which should be related to the different magnetic induction at increasing and decreasing fields, due to the critical state. As discussed in Sec. 4, the increasing-field branch of the $R_s(H_0)$ curve should exhibit a change of concavity, from positive to negative, when the external magnetic field reaches the full penetration field, H^* . By considering the sample width and the value of J_c at $T = 5$ K reported for sample P0 [13], the expected value of H^* is ≈ 2.6 T. Nevertheless, we observe a negative concavity of the $R_s(H_0)$ increasing-field branch in the whole range of fields investigated (see Fig. 3a), even if the maximum value of the applied field is well below H^* . The decreasing-field branch should show a monotonic reduction of R_s down to low fields. In contrast, for $H_0 < H'$, we observe an initial weak reduction followed by a plateau, from $\mu_0 H_0 \approx 0.2$ T down to zero. The presence of this plateau is puzzling because it would suggest that the trapped flux does not change anymore on decreasing the field below ~ 0.2 T, although this value is four times larger than H_p .

Another anomalous result concerns the range of magnetic fields in which we observe the hysteretic behavior. As we have already mentioned, we have experienced that for samples of millimetric size the sensitivity of our experimental apparatus allows detecting hysteresis in $R_s(H_0)$ for $J_c \gtrsim 10^4$ A/cm². From Fig. 9 of Ref. [13], one can deduce that, in sample P0, such condition occurs at $\mu_0 H_0 \sim 4$ T; so, we should detect hysteresis in the whole range of fields we have investigated. On the contrary, we obtained $H'(4.2$ K) ~ 0.5 T, one order of magnitude lower than the expected value.

We would like to remark that these anomalies have been observed in all the bulk MgB₂ samples (unirradiated) we have investigated, no matter the preparation method and the components (¹¹B or ¹⁰B) used in the synthesis process [38,40]. The finding that in sample P6 the experimental results are fully justified by the used model, strongly suggests that these anomalies are strictly related to the presence of the two superconducting gaps.

At temperatures close to T_c and for $H_0 \gtrsim 0.5H_{c2}(T)$, the experimental results can be accounted for by the model discussed in Sec. 4, provided that the anisotropy of the upper critical field is taken into due account. Following Ref. [14], to take into account the anisotropy, we have assumed that the polycrystalline sample is constituted by grains with the c -axis randomly oriented with respect to the DC-magnetic-field direction; so, the distribution of their orientations follows a $\sin(\theta)$ law, being θ the angle between \mathbf{H}_0 and $\hat{\mathbf{c}}$. Furthermore, we have used for the angular dependence of the upper critical field the anisotropic Ginzburg-Landau relation

$$H_{c2}(\theta) = \frac{H_{c2}^{\perp c}}{\sqrt{\gamma^2 \cos^2(\theta) + \sin^2(\theta)}},$$

where $\gamma = H_{c2}^{\perp c}/H_{c2}^{\parallel c}$ is the anisotropy factor.

The field-induced variations of R_s observed at $T = 38$ K (reported in Fig. 5a) do not exhibit hysteresis; so, in this case, B can be considered uniform. Furthermore, at temperatures near T_c , one can reasonably suppose fluxons move in the flux-flow regime. In this condition, the expected $R_s(H_0, H_{c2}(\theta))$ curve depends on λ_0/δ_0 (obtained by fitting the $R_s(T)$ curve at $H_0 = 0$), $H_{c2}^{\perp c}$ and γ . On the other hand, the H_{c2} values deduced from the isothermal $R_s(H_0)$ curves (see Fig. 6b) coincide with the magnetic field at which the whole sample goes to the normal state, i.e. $H_{c2}^{\perp c}$. In order to fit the results at $T = 38$ K, we have averaged the expected curve [calculated by Eqs. (1–4)] over a $\sin(\theta)$ distribution, have used for $H_{c2}^{\perp c}$ the value of the magnetic field at which $R_s/R_n = 1$, letting it vary within the experimental uncertainty, have taken γ as free parameter. At this value of temperature, the experimental results can be accounted for using $\gamma = 3.3 \pm 0.5$. In particular, the best-fit curve reported in Fig. 5a has been obtained with $\gamma = 3.3$ and $\mu_0 H_{c2}^{\perp c} = 145$ mT. As one can see, the field-induced variation of R_s is well described by the model of Sec. 4. We think that this occurs because at this temperature the superfluid fraction of the π band is strongly suppressed at low magnetic fields, the flux line gets a conventional structure and the fluxon dynamics can be described by standard models.

Prompted by the results obtained at $T = 38$ K, we have tried to fit the experimental data obtained in the temperature range $34 \div 37$ K by the same method (for these temperatures, the upper critical field has been directly deduced from the $R_s(H_0)$ curves). Since in this temperature range we have detected magnetic hysteresis, we have considered only the reversible part of the $R_s(H_0)$ curve. In order to fit the data, we have hypothesized fluxons move in the flux-flow regime, have considered

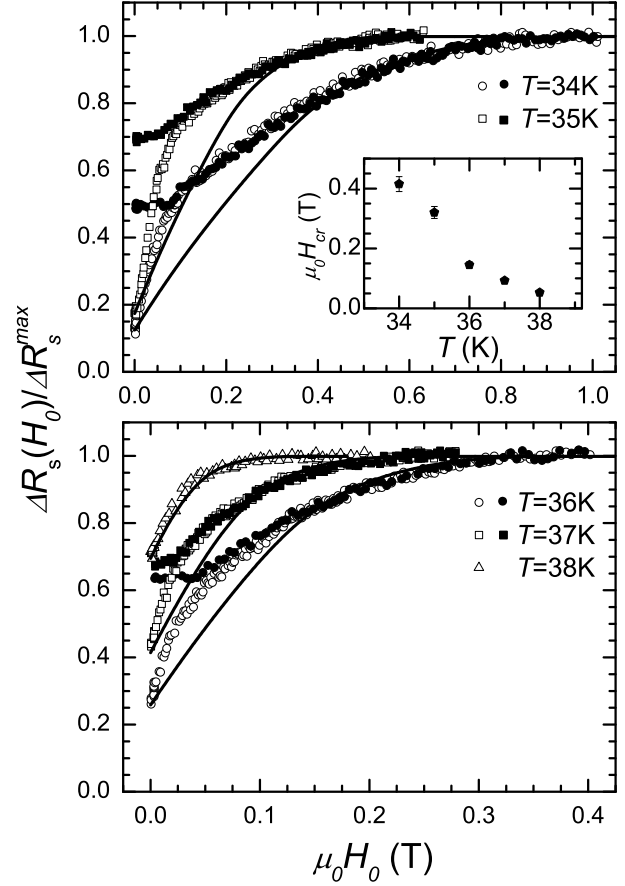


Fig. 10. Normalized field-induced variations of R_s for sample P0, at different temperatures near T_c . Open symbols are the results obtained at increasing H_0 , full symbols those at decreasing H_0 . The $R_s(H_0)$ curve at $T = 38$ K is reversible. The lines are the expected curves, obtained with $\gamma = 2.6$ as described in the text. The inset shows the temperature dependence of the magnetic field H_{cr} , above which the experimental data can be justified in the framework of the model of Sec. 4.

for $H_{c2}^{\perp c}(T)$ the values reported in the inset of Fig. 6b, letting them vary within the experimental uncertainty, and have taken γ as fitting parameter. We have found that at high fields the experimental results can be fitted using $\gamma = 2.6 \pm 0.2$. Fig. 10 shows a comparison between the expected curves, obtained with $\gamma = 2.6$, and the experimental data for $T = 34 \div 38$ K; open symbols are the results obtained at increasing H_0 , full symbols those at decreasing H_0 . As one can see, the expected $R_s(H_0)$ curve at $T = 38$ K so obtained poorly agrees with the experimental data at low fields; on the contrary, the line of Fig. 5a, which has been obtained with $\gamma = 3.3$, fits the data in the whole range of magnetic fields. However, the value $\gamma = 2.6$ is closer to the upper-critical-field anisotropy reported in the literature for MgB₂ at temperatures near T_c [5, 23, 45, 46].

The results of Fig. 10 show that for H_0 greater than a certain threshold value, depending on T , the data can be justified in the framework of the model describing the fluxon dynamics of conventional vortex lattice. The tem-

perature dependence of the threshold field, H_{cr} , is reported in the inset. For $H_0 < H_{cr}$ the field-induced mw losses are larger than those expected for single-gap superconductors in the mixed state. We suggest that this surplus of mw losses is due to the additional contribution of π -band quasiparticles within the vortex cores with respect to that of one-gap superconductors; the finding that H_{cr} decreases on increasing T seems to support this hypothesis. It is easy to see that the $H_{cr}(T)$ values coincide, within the experimental uncertainty, with $0.5H_{c2}(T)$ (see the inset of Fig. 6). Presently, it is not clear why just above $0.5H_{c2}$ the results can be justified by a standard model, which does not consider the two-gap nature of MgB₂. Furthermore, we remark that H_{cr} cannot be identified with the magnetic field at which the π -band superfluid is suppressed; indeed several authors have reported $H_{c2}^{\pi} \sim 0.1H_{c2}^{\perp c}$ [1, 3, 22, 23, 24, 25].

6 Conclusions

We have investigated the microwave surface resistance at 9.6 GHz of two polycrystalline Mg¹¹B₂ samples prepared by direct synthesis from Mg (99.999% purity) and crystalline isotopically enriched ¹¹B (99.95% purity). That labelled as P0 consists of pristine material; the other, labelled as P6, has been exposed to neutron irradiation at very high fluence. Several superconducting properties of these samples have been reported in Refs. [13, 14, 15, 16, 17]. Point-contact spectroscopy and specific-heat measurements, have shown that sample P0 exhibits a clear two-gap-superconductivity behavior; in sample P6 the irradiation process determined a merging of the two gaps into a single value. To our knowledge, the mw response of neutron irradiated MgB₂ samples has not yet been investigated.

The mw surface resistance has been measured as a function of the temperature and the DC magnetic field. By measuring the field-induced variations of R_s at increasing and decreasing fields we have detected a magnetic hysteresis ascribable to the critical state of the fluxons lattice. The range of temperatures in which the hysteretic behavior has been observed is different for the two samples; in the irradiated sample the hysteresis is undetectable at $T/T_c \gtrsim 0.55$ while in the unirradiated sample it is detectable up to $T/T_c \approx 0.95$.

The results obtained in the irradiated sample have been quite well justified in the framework of the Coffey and Clem model with the normal fluid density following the Gorter and Casimir two-fluid model. In order to account for the hysteretic behavior, we have used a generalized Coffey and Clem model in which we take into account the non-uniform fluxon distribution due to the critical state.

The peculiarities of the mw surface resistance of sample P0 differ from those observed in sample P6, in both the temperature and the field dependencies. The $R_s(T)$ curve obtained at zero field shows a wide tail, from $T/T_c \approx 0.9$ down to $T/T_c \approx 0.7$, which cannot be justified in the framework of the Gorter and Casimir two-fluid model. We

have shown that, in order to account for this behavior, it is essential to hypothesize a linear temperature dependence of the normal and condensed fluid densities. Such finding agrees with the experimental temperature dependence of the penetration depth reported in the literature, which have been justified in the framework of two-gap models for the MgB₂ superconductor.

The $R_s(H_0)$ curves in sample P0 have shown several anomalies, especially at low temperatures, among which an enhanced field-induced variation and a magnetic hysteresis of unconventional shape. At low temperatures, a magnetic field $H_0 \approx H_{c2}/15$ causes a R_s variation of $\approx 35\%$ of the normal-state value. We remark that in sample P6 a variation of the same order of magnitude is obtained for $H_0 \approx H_{c2}/2$. The shape of the magnetic hysteresis, which has been observed in a wide range of temperatures below T_c , cannot be justified in the framework of the critical-state models; the most unexpected behavior concerns the decreasing-field branch, in which we observed a plateau extending from $\mu_0 H_0 \sim 0.2$ T down to zero. The presence of this plateau is puzzling because it would suggest that the trapped flux does not change anymore on decreasing the field below 0.2 T, although this value is four times larger than the first penetration field.

The investigation at temperatures near T_c has highlighted that, in the range $T = 34 \div 38$ K, the results obtained in sample P0 for $H_0 \gtrsim 0.5H_{c2}$ can be justified in the framework of the Coffey and Clem model taking into account the anisotropy of the upper critical field. We suggest that this occurs because at these field values the superfluid fraction of the π band is strongly suppressed, the flux line gets a conventional structure and the fluxon dynamics can be described by standard models.

The enhanced field-induced variation of R_s , observed at low T in the whole range of fields investigated as well as at $T \sim T_c$ for $H_0 \lesssim 0.5H_{c2}$, may be qualitatively ascribed to the presence and motion of the giant cores due to the π -band quasiparticles. On the contrary, the origin of the anomalous shape of the $R_s(H_0)$ curve is so far not understood. We would like to remark that the results we obtained in sample P0 are very similar to those, not reported here, we have obtained in several MgB₂ samples (unirradiated), no matter the preparation method and the components (¹¹B or ¹⁰B) used in the synthesis process. The comparison between the results obtained in the two samples here investigated strongly suggest that the anomalies in the $R_s(H_0)$ curves are related to the unusual structure of fluxons due to the two superconducting gaps. According to what suggested by different authors, our results confirm that the standard models are inadequate to describe the fluxon dynamics in two-gap MgB₂. Further investigation is necessary for understanding how to take into account the complex vortex structure in describing the fluxon dynamics in MgB₂.

Acknowledgements

The authors are very glad to thank D. Daghero, G. Ghigo, R. S. Gonnelli and M. Putti for their interest to this work

and helpful suggestions; G. Lapis and G. Napoli for technical assistance.

References

1. A. V. Sologubenko, J. Jun, S. N. Kazakov, J. Karpinski, H. R. Ott, Phys. Rev. B **65**, 180505 (2002); *ibid.* **66**, 014504 (2002).
2. B. B. Jin, N. Klein, W. N. Kang, H.-J. Kim, E.-M. Choi, S.-I. Lee, T. Dahm, K. Maki, Phys. Rev. B **66**, 104521 (2002).
3. F. Bouquet, Y. Wang, I. Sheikin, T. Plackovski, A. Junod, Phys. Rev. Lett. **89**, 257001 (2002).
4. A. Gurevich, Phys. Rev. B **67**, 184515 (2003).
5. A. A. Golubov, A. E. Koshelev, Phys. Rev. B **68**, 104503 (2003).
6. A. A. Golubov, A. Brinkman, O. V. Dolgov, J. Kortus, O. Jepsen, Phys. Rev. B **66**, 054524 (2002).
7. A. Y. Liu, I. I. Mazin, J. Kortus, Phys. Rev. Lett. **87**, 087005 (2001).
8. I. I. Mazin, O. K. Andersen, O. Jepsen, O. V. Dolgov, J. Kortus, A. A. Golubov, A. B. Kuz'menko, D. van der Marel, Phys. Rev. Lett. **89**, 107002 (2002).
9. R. H. T. Wilke, S. L. Bud'ko, P. C. Canfield, D. K. Finnemore, R. J. Suplinskas, S. T. Hannahs, Physica C **424**, 1 (2005).
10. R. H. T. Wilke, S. L. Bud'ko, P. C. Canfield, J. Farmer, and S. T. Hannahs, Phys. Rev. B **73**, 134512 (2006).
11. R. Gandikota, R. K. Singh, J. Kim, B. Wilkens, N. Newman, J. M. Rowell, A. V. Pogrebnyakov, X. X. Xi, J. M. Redwing, S. Y. Xu, Q. Li, B. H. Moeckly, Appl. Phys. Lett. **86**, 012508 (2005); *ibid.* **87**, 072507 (2005).
12. G. Ghigo, G. A. Ummarino, R. Gerbaldo, M. Gozzelino, F. Laviano, and E. Mezzetti, Phys. Rev. B **74**, 184518 (2006).
13. C. Tarantini, H. U. Aebersold, V. Braccini, G. Celentano, C. Ferdeghini, V. Ferrando, U. Gambardella, F. Gatti, E. Lehmann, P. Manfrinetti, D. Marré, A. Palenzona, I. Pallecchi, I. Sheikin, A. S. Siri, M. Putti, Phys. Rev. B **73**, 134518 (2006), and Refs. therein.
14. I. Pallecchi, C. Tarantini, H. U. Aebersold, V. Braccini, C. Fanciulli, C. Federghini, F. Gatti, E. Lehman, P. Manfrinetti, D. Marré, A. Palenzona, A. S. Siri, M. Vignolo, M. Putti, Phys. Rev. B **71**, 212507 (2005).
15. D. Daghero, A. Calzolari, G. A. Ummarino, M. Tortello, R. S. Gonnelli, V. A. Stephanov, C. Tarantini, P. Manfrinetti, E. Lehamann, Phys. Rev. B **74**, 174519 (2006).
16. M. Putti, M. Affronte, C. Federghini, P. Manfrinetti, C. Tarantini, E. Lehmann, Phys. Rev. Lett. **96**, 077003 (2006).
17. A. Martinelli, C. Tarantini, E. Lehmann, P. Manfrinetti, A. Palenzona, I. Pallecchi, M. Putti, C. Ferdeghini, Supercond. Sci. Technol. **21**, 012001 (2008).
18. M. Zehetmayer, M. Eisterer, J. Jun, S. M. Kazakov, J. Karpinski, H. W. Weber, Phys. Rev. B **70**, 214516 (2004).
19. Y. Jia, Y. Huang, H. Yang, L. Shan, C. Ren, C. G. Zhuang, Y. Cui, Qi Li, Z. K. Liu, X. X. Xi, H. H. Wen, arXiv:cond-mat/0703637.
20. H. Yang, Y. Jia, L. Shan, Y. Zhang, H. H. Wen, C. G. Zhuang, Z. K. Liu, Qi Li, Y. Cui, X. X. Xi, Phys. Rev. B **76**, 134513 (2007).
21. A. E. Koshelev, A. A. Golubov, Phys. Rev. Lett. **90**, 177002 (2003).
22. M. R. Eskildsen, M. Kugler, S. Tanaka, J. Jun, S. M. Kazakov, J. Karpinski, ø. Fisher, Phys. Rev. Lett. **89**, 187003 (2002).
23. R. Cubitt, S. Levett, S. L. Bud'ko, N. E. Anderson, P. C. Canfield, Phys. Rev. Lett. **90**, 157002 (2003); R. Cubitt, M. R. Eskildsen, C. D. Dewhurst, J. Jun, S. M. Kazakov, J. Karpinski, Phys. Rev. Lett. **91**, 047002 (2003).
24. P. Samuely, P. Szabó, J. Kacmarcik, T. Klein, A. G. M. Jansen, Physica C **385**, 244 (2003).
25. D. Daghero, R. S. Gonnelli, G. A. Ummarino, V. A. Stephanov, J. Jun, S. M. Kazakov, J. Karpinski, Physica C **355**, 255 (2003).
26. Y. Bogoslavsky, Y. Miyoshi, G. K. Perkins, A. D. Kaplin, L. F. Cohen, A. V. Progrebnyakov, X. X. Xi, Phys. Rev. B **72**, 224506 (2005).
27. M. Golosovsky, M. Tsindlekht, D. Davidov, Supercond. Sci. Technol. **9**, 1 (1996) and Refs. therein.
28. J. Owliaei, S. Shridar, J. Talvacchio, Phys. Rev. Lett. **69**, 3366 (1992).
29. S. Fricano, M. Bonura, A. Agliolo Gallitto, M. Li Vigni, L. A. Klinkova, N. V. Barkovskii, Eur. Phys. J. B **41**, 313 (2004).
30. M. W. Coffey, J. R. Clem, Phys. Rev. Lett. **67**, 386 (1991); Phys. Rev. B **45**, 9872 (1992); **45**, 10527 (1992).
31. E. H. Brandt, Phys. Rev. Lett. **67**, 2219 (1991).
32. A. Dulčić, M. Požek, Physica C **218**, 449 (1993).
33. S. Y. Lee, J. H. Lee, J.H. Han, S. H. Moon, H. N. Lee, J. C. Booth, J. H. Claassen, Phys. Rev. B **71**, 104514 (2005).
34. E. Di Gennaro, G. Lamura, A. Palenzona, M. Putti, A. Andreone, Physica C **408-410**, 125 (2004).
35. A. Shibata, M. Matsumoto, K. Izawa, Y. Matsuda, S. Lee, S. Tajima, Phys. Rev. B **68**, 060501(R) (2003).
36. A. Dulčić, D. Paar, M. Požek, V. M. Williams, S. Krämer, C. U. Jung, Min-Seok Park, Sung-Ik Lee, Phys. Rev. B **66**, 014505 (2002).
37. A. Agliolo Gallitto, G. Bonsignore, S. Fricano, M. Guccione, M Li Vigni, *Topics in Superconductivity Research*, B. P. Martins Ed., Nova Science Publishers, Inc. (New York 2005), pags. 125-143.
38. A. Agliolo Gallitto, M. Bonura, S. Fricano, M. Li Vigni, G. Giunchi, Physica C **404**, 171 (2003).
39. S. Sarti, C. Amabile, E. Silva, M. Giura, R. Fastampa C. Ferdeghini, V. Ferrando, C. Tarantini, Phys. Rev. B **72**, 024542 (2005). E. Silva, N. Pompeo, S. Sarti, C. Amabile, arXiv:cond-mat/0607676v1.
40. A. Agliolo Gallitto, M. Bonura, M. Li Vigni, J. Phys: Conf. Series, in press; arXiv:cond-mat/0709.0840.
41. J. M. Rowell, Supercond. Sci. Technol. **16**, R17 (2003).
42. M. Bonura, A. Agliolo Gallitto, M. Li Vigni, Eur. Phys. J. B **53**, 315 (2006), and Refs. therein.
43. S. L. Li, H. H. Wen, Z. W. Zhao, Y. M. Ni, Z. A. Ren, G. C. Che, H. P. Yang, Z. Y. Liu, Z. X. Zhao, Phys. Rev. B **64**, 094522 (2001).
44. A. Sharoni, I. Felner, O. Millo, Phys. Rev. B **63**, 220508(R) (2001).
45. A. D. Caplin, Y. Bugoslavsky, L. F. Cohen, L. Cowey, J. Driscoll, J. Moore, G. K. Perkins, Supercond. Sci. Technol. **16**, 176 (2003).
46. L. Lyard, P. Szabó, T. Klein, J. Marcus, C. Marcenat, K. H. Kim, B. W. Kang, H. S. Lee, S. I. Lee, Phys. Rev. Lett. **92**, 57001 (2004).
47. E. H. Brandt, G. P. Mikitik, Phys. Rev. Lett. **89**, 027002 (2002); G. P. Mikitik, E. H. Brandt, Phys. Rev. B **67**, 104511 (2003).

48. M. Bonura, E. Di Gennaro, A. Agliolo Gallitto, M. Li Vigni, *Eur. Phys. J. B* **52**, 459 (2006).
49. C. P. Moca, *Phys. Rev. B* **65**, 132509 (2002).
50. A. G. Zaitsev, R. Schneider, R. Hott, Th. Schwarz, and J. Geerk, *Phys. Rev. B* **75**, 212505 (2007)